

# Hidden antiferro-nematic order in Fe-based superconductor $\text{BaFe}_2\text{As}_2$ and $\text{NaFeAs}$ above $T_S$

Seiichiro Onari and Hiroshi Kontani

Department of Physics, Nagoya University, Furo-cho, Nagoya 464-8602, Japan.

(Dated: November 26, 2019)

In some Fe-based superconductors,  $C_4$  symmetry breaking occurs at  $T^*$ , which is tens of Kelvin higher than the structural transition temperature  $T_S$ . In this “hidden” nematic state at  $T_S < T < T^*$ , the orthorhombicity is tiny [ $\phi = (a - b)/(a + b) \ll 0.1\%$ ], but clear evidences of bulk phase transition have been accumulated. To explain this long-standing mystery, we propose the emergence of antiferro-bond (AFB) order with the antiferro wavevector  $\mathbf{q} = (0, \pi)$  at  $T = T^*$ , by which the characteristic phenomena below  $T^*$  are satisfactorily explained. This AFB order originates from the inter-orbital nesting between the  $d_{xy}$ -orbital hole-pocket and the electron-pocket, and this inter-orbital order naturally explains the pseudogap, band-folding, and tiny nematicity that is linear in  $T^* - T$ . The AFB order at  $T^*$  does not interrupt the ferro-orbital order at  $T_S$  owing to the difference in the orbital selectivity. In addition, we discuss the significant role of AFB fluctuations on the pairing mechanism in Ba122 families.

The emergence of rich nematic phase transitions is a central unsolved issue in Fe-based superconductors. At the structural transition temperature  $T_S$ , ferro-orbital (FO) order with  $\psi \equiv (n_{xz} - n_{yz})/(n_{xz} + n_{yz}) \neq 0$  is driven by electron correlation [1], by which the orthorhombicity  $\phi = (a - b)/(a + b)$  occurs in proportion to  $\psi$ . Above  $T_S$ , the electronic nematic susceptibility develops divergently[2–5]. As possible mechanisms of nematicity, both spin-nematic scenarios [6–12] and the orbital/charge-order scenarios [13–24] have been proposed. However, the nematicity in Fe-based superconductors was recently reported to exhibit very rich variety beyond the original expectation. Famous discoveries are the nematicity without magnetization in FeSe and the nematicity with  $B_{2g}$  symmetry in the heavily hole-doped compound  $\text{AFe}_2\text{As}_2$  ( $\text{A}=\text{Cs, Rb}$ ) [25–28], which is rotated by  $45^\circ$  with respect to the nematicity in FeSe. These nematic orders are naturally understood as the spin-fluctuation-driven bond-order described by the Aslamazov–Larkin (AL) and Maki–Thompson (MT) vertex corrections (VCs) [17].

The most significant open issue in the nematicity is the emergence of another nematicity in various Ba122 compounds below  $T = T^*$ , which is higher than  $T_S$  by tens of Kelvin. A true second-order bulk nematic transition at  $T^*$  has been reported in many experimental studies, such as a magnetic torque study[29], an X-ray study[30], an optical measurement study[31], and a laser Photoemission electron microscope study[32].

Below  $T^*$ , the orthorhombicity  $\phi$  is finite but very small ( $\ll 0.1\%$ ), but a sizable pseudogap and the shadow band exist[33, 34]. The exponent of the nematicity  $\psi \propto \phi \propto (T^* - T)^\alpha$  is  $\alpha \sim 1$ , which is much larger than the mean-field exponent (1/2). The relation  $\phi \propto (T^* - T)$  is also observed in NaFeAs[35]. One may consider that the nematicity at  $T^*$  is not a true phase transition, but reflects the inhomogeneity of the FO-order transition temperature  $T_S$  due to local uniaxial pressure and

randomness [7, 36, 37]. On the other hand,  $T^*$  seems to be insensitive to the sample quality, and the domain structure of nematicity observed in the  $C_4$  phase above  $T_S$ [31, 32] is homogeneous. The aim of this study is to reveal the origin of this mysterious hidden nematic state below  $T = T^*$ , and to explain why multistage-nematic transitions (at  $T = T^*$  and  $T_S$ ) emerge in Ba122 and NaFeAs families.

In this paper, we predict the emergence of antiferro-bond (AFB) order with the antiferro wavevector  $\mathbf{q} = (0, \pi)$  at  $T = T^*$ , above the FO-order transition temperature  $T_S$ . Below  $T^*$ , the AFB order causes a pseudogap in the density of states and the small  $T$ -linear nematicity  $\psi \propto T^* - T$ . The AFB order does not interrupt the ferro-orbital order at  $T_S$ , because these order parameters have different orbital components. Thus, both the spin and nematic susceptibilities,  $\chi^s(\mathbf{Q})$  and  $\chi_{\text{nem}}(\mathbf{0})$ , respectively, show only a small anomaly at  $T = T^*$ . The inter-orbital order below  $T^*$  is driven by the higher-order VCs in the presence of inter-orbital nesting between  $d_{xy}$ -orbital hole-pocket and electron-pockets. The present theory naturally explains the long-standing mystery of the hidden nematic state below  $T^*$  in Ba122 and NaFeAs families, in both of which  $T$ -linear nematicity has been reported[29, 35]. Finally, we discuss the significant role of the AFB fluctuations on the superconducting pairing mechanism. The  $s_{++}$ -wave state without sign reversal is favored by the AFB fluctuations, which is the extensive of the previous charge quadrupole mechanism[16].

Below, we denote the five  $d$ -orbitals  $d_{3z^2-r^2}$ ,  $d_{xz}$ ,  $d_{yz}$ ,  $d_{xy}$ , and  $d_{x^2-y^2}$  as  $l = 1, 2, 3, 4$ , and 5, respectively. We analyze the following two-dimensional eight-orbital  $d$ - $p$  Hubbard model with parameter  $r$  [19]:

$$H_M(r) = H^0 + r H^U, \quad (1)$$

where  $H^0$  is the unfolded tight-binding model for  $\text{BaFe}_2\text{As}_2$  [38] or FeSe [19]; more details are presented in Supplementary Material (SM) A [39]. Furthermore,

$H^U$  is the first-principles screened Coulomb potential for  $d$ -electrons[40], and  $r$  is the reduction parameter. Figure 1(a) shows the unfolded Fermi surfaces (FSs) in the  $\text{BaFe}_2\text{As}_2$  model. The size of h-FS3 around M point composed of orbital 4 is similar to that of e-FS1(2) around X(Y) point, which results in a good inter-orbital nesting. On the other hand, h-FS3 is missing among the FSs in the FeSe model shown in Fig. 1(b).

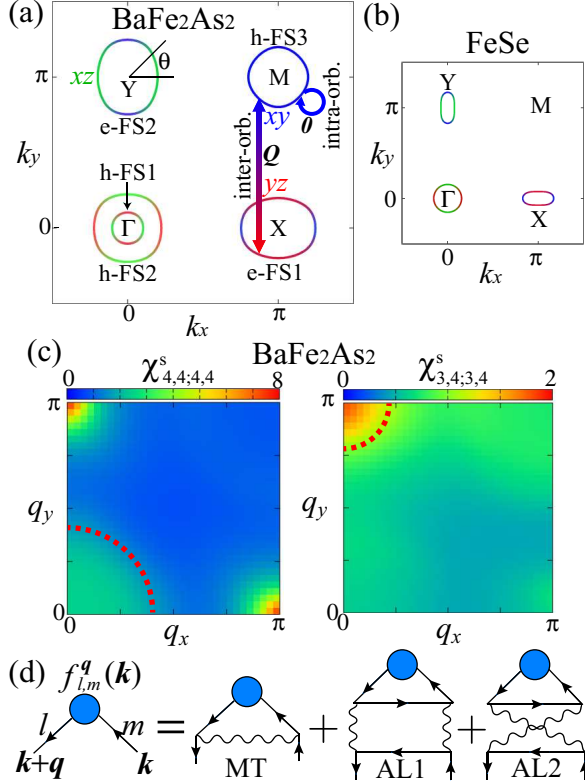


FIG. 1: (a) FSs of the  $\text{BaFe}_2\text{As}_2$  model in the unfolded zone. The colors green, red and blue correspond to orbitals 2, 3, and 4, respectively. We depict the inter-orbital interaction due to the nesting  $\mathbf{Q} = (0, \pi)$  between h-FS3 (orbital 4) and e-FS1 (orbital 3) as well as the forward intra-orbital interaction for orbital 4 at M.  $\theta$  denotes an azimuthal angle from the x axis on each FS. (b) FSs of the FeSe model in the unfolded zone. (c)  $\mathbf{q}$  dependences of  $\chi_{4,4;4,4}^s(\mathbf{q}, 0)$  and  $\chi_{3,4;3,4}^s(\mathbf{q}, 0)$  given by the RPA in the  $\text{BaFe}_2\text{As}_2$  model. The large antiferro- and ferro-fluctuations denoted by dotted circles are significant for the AFB order formation. (d) Feynman diagrams of the DW equation. Each wavy line represents a fluctuation-mediated interaction.

We calculate the spin (charge) susceptibilities  $\hat{\chi}^{s(c)}(q)$  for  $q = (\mathbf{q}, \omega_m = 2m\pi T)$  based on the random-phase-approximation (RPA). The spin Stoner factor  $\alpha_s$  is defined as the maximum eigenvalue of  $\hat{\Gamma}^s \hat{\chi}^0(\mathbf{q}, 0)$ , where  $\hat{\Gamma}^{s(c)}$  is the bare Coulomb interaction for the spin (charge) channel, and  $\hat{\chi}^0$  is the irreducible susceptibilities given by the Green function without self-energy  $\hat{G}(k) = [(i\epsilon_n - \mu)\hat{1} - \hat{h}^0(\mathbf{k})]^{-1}$  for  $k = [\mathbf{k}, \epsilon_n = (2n + 1)\pi T]$ . Here,  $\hat{h}^0(\mathbf{k})$  is the matrix expression of  $H^0$  and  $\mu$  is the chemical po-

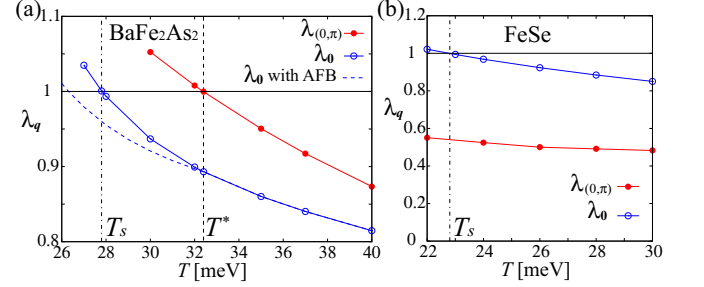


FIG. 2:  $T$  dependences of  $\lambda_q$  for  $\mathbf{q} = \mathbf{0}$  and  $\mathbf{q} = (0, \pi)$  in (a) the  $\text{BaFe}_2\text{As}_2$  model and in (b) the FeSe model for  $r = 0.239$ . The blue dotted line shows  $\lambda_0$  with the AFB order for  $T < T^*$ .

tential. Details of  $\hat{\Gamma}^{s(c)}$ ,  $\hat{\chi}^{s(c)}(q)$ , and  $\hat{\chi}^0(q)$  are presented in SM A [39]. We use  $N = 64 \times 64$   $\mathbf{k}$ -meshes and 512 Matsubara frequencies, and fix the parameters  $r = 0.303$  in the  $\text{BaFe}_2\text{As}_2$  model unless otherwise noted. Figure 1(c) shows the obtained spin susceptibilities  $\chi_{4,4;4,4}^s(\mathbf{q}, 0)$  and  $\chi_{3,4;3,4}^s(\mathbf{q}, 0)$  for  $\alpha_s = 0.951$  at  $T = 32.4$  meV in the  $\text{BaFe}_2\text{As}_2$  model. They have peak at  $\mathbf{q} = (0, \pi)$  due to the intra-orbital (4-4) or the inter-orbital (3-4) nesting. The FSs of NaFeAs are similar to those in Fig. 1(a).  $\chi_{4,4;4,4}^s$  is larger than  $\chi_{3,3;3,3}^s$  because the intra- $d_{xy}$ -orbital nesting between e-FS1,2 and h-FS3 is better than the intra- $d_{yz}$ -orbital nesting between e-FS2 and h-FS1,2.

Hereafter, we study the symmetry breaking in the self-energy  $\hat{f}^q$  for wavevector  $\mathbf{q}$  based on the density-wave (DW) equation introduced in Ref. [19, 28, 41]. We calculate both the momentum and orbital dependences of  $\hat{f}$  self-consistently to analyze both the orbital order and bond order on equal footing. To identify the realized DW with wavevector  $\mathbf{q}$ , we solve the following linearized DW equation:

$$\lambda_q f_{l,l'}^q(k) = \frac{T}{N} \sum_{k',m,m'} K_{l,l';m,m'}^q(k, k') f_{m,m'}^q(k'), \quad (2)$$

where  $\lambda_q$  is the eigenvalue of the DW equation. The DW with wavevector  $\mathbf{q}$  appears when  $\lambda_q = 1$ , and the eigenvector  $\hat{f}^q(k)$  gives the DW form factor. Details of the kernel function  $\hat{K}^q(k, k')$  are given in SM A [39]. The MT terms and AL terms are included in the kernel function, as shown by the Feynman diagrams in Fig. 1(d). Near the magnetic criticality, the AL terms are strongly enhanced in proportion to  $\sum_p \chi^s(p) \chi^s(p+q)$ , resulting in strong charge-spin mode coupling. Thus, the AL terms cause the spin-fluctuation-driven DW order.

Figure 2 (a) shows the  $T$  dependencies of eigenvalue  $\lambda_q$  for  $\mathbf{q} = \mathbf{0}$  FO order and  $\mathbf{q} = (0, \pi)$  AFB order.  $\lambda_{(0,\pi)}$  reaches 1 at  $T^* = 32.4$  meV, and  $\lambda_0$  reaches 1 at  $T_S = 27.8$  meV successively in the  $\text{BaFe}_2\text{As}_2$  model. Thus, the AFB order is expected to emerge as the hidden nematic state at  $T^*(> T_S)$ . The blue dotted line in Fig. 2(a) shows  $\lambda_0$  under the AFB order for  $T < T^*$ .  $\lambda_0$  is suppressed only slightly by the AFB order owing

to the orbital selectivity in nematicity, that is, the FO-order and AFB-order parameters have different orbital component. Details are given in SM B and C [39]. On the other hand, AFB order is absent in the FeSe model because  $\lambda_{(0,\pi)}$  is always less than  $\lambda_0$ , as shown in Fig. 2(b). This result is consistent with the absence of the hidden nematic order in FeSe[42].

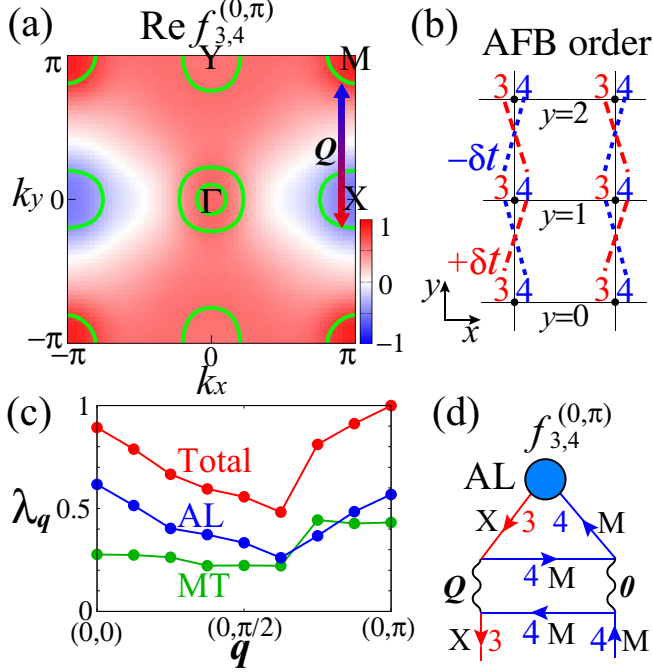


FIG. 3: (a) Dominant form factor of the off-diagonal orbitals 3 and 4 for  $\mathbf{q} = (0, \pi)$  obtained as the largest eigenvalue in the  $\text{BaFe}_2\text{As}_2$  model. The green lines indicate FSs. (b) Schematic picture of inter-orbital AF-bond (AFB) order (staggered along the  $y$  direction) induced by  $f_{3,4}^{(0,\pi)}$ . (c)  $\mathbf{q}$  dependences of  $\lambda_q$  for all the VC terms, AL terms, and MT terms in the  $\text{BaFe}_2\text{As}_2$  model. (d) Dominant Feynman diagram of the AL term for AFB  $f_{3,4}^{(0,\pi)}$ .

From the solution  $\hat{f}^{\mathbf{q}}(\mathbf{k})$  of the DW equation, we derive the static form factor  $\hat{f}^{\mathbf{q}}(\mathbf{k})$  at  $\epsilon = 0$  based on analytic continuation. Figure 3(a) shows the dominant form factor  $f_{3,4}^{\mathbf{q}}(\mathbf{k})$  for  $\mathbf{q} = (0, \pi)$  obtained in the  $\text{BaFe}_2\text{As}_2$  model, which is normalized as  $\max_{\mathbf{k}} |f_{3,4}^{(0,\pi)}(\mathbf{k})| = 1$ . Other sub-dominant components are shown in SM B [39]. Focusing on the X and M points,  $f_{3,4}^{(0,\pi)}(\mathbf{k})$  is proportional to  $-\cos(k_y)$ , which corresponds to the inter-orbital AFB order, where the  $y$ -direction hoppings between orbitals 3 and 4 are modulated by the correlation hopping  $\delta t_{3,4}(y; y \pm 1) = -\delta t_{4,3}(y; y \pm 1) = \delta t(-1)^y$  as shown in Fig. 3(b). Note that  $\delta t_{l,m}(y; y') \equiv \delta t_{m,l}(y'; y)$ .

$f_{3,4}^{(0,\pi)}$  is closely related to the inter-orbital nesting  $\mathbf{Q} = (0, \pi)$  between orbitals 3 in e-FS1 and orbital 4 in h-FS3 as well as the forward intra-orbital interaction of orbital 4 in h-FS3, as shown in Fig. 1(a). In order

to clarify the origin of the inter-orbital AFB order, we show the contributions from the MT term and AL term to the total  $\lambda_q$  separately in Fig. 3(c). We see that the contribution from the AL term is dominant at  $\mathbf{q} \sim \mathbf{0}$  and  $\mathbf{q} \sim (0, \pi)$ , while the contribution from the MT term is large only at  $\mathbf{q} \sim (0, \pi)$ . Figure 3(d) shows the dominant AL term for the form factor  $f_{3,4}^{(0,\pi)}(\mathbf{k})$ , where  $\mathbf{k}$  is on h-FS3 (orbital 4) and  $\mathbf{k} + \mathbf{Q}$  is on e-FS1 (orbital 3). The enhancement of the AL term is mainly due to the product of  $\chi_{3,4;3,4}^s(\mathbf{Q})$  and  $\chi_{4,4;4,4}^s(\mathbf{0})$  for  $\mathbf{Q} \sim (0, \pi)$  because both fluctuations develop as shown by the red dotted circle in Fig. 1(c). Furthermore, the MT term induces the sign change of  $f_{3,4}^{(0,\pi)}(\mathbf{k})$  between X and M points, as indicated by previous studies[19, 28, 43]. Thus, the AFB order originates from the cooperation between the AL and MT terms due to the inter-orbital nesting between h-FS3 and e-FS1. This is consistent with the presence of  $T^*$  in Ba122 and NaFeAs with inter-orbital nesting between e-FS1 and h-FS3, as well as the absence of  $T^*$  in FeSe, where h-FS3 is missing. As discussed in previous papers[17, 18, 20], the FO order originates from the AL term including  $\chi_{3,3;3,3}^s(\mathbf{Q}')$  for  $\mathbf{Q}' = (\pi, 0)$ .

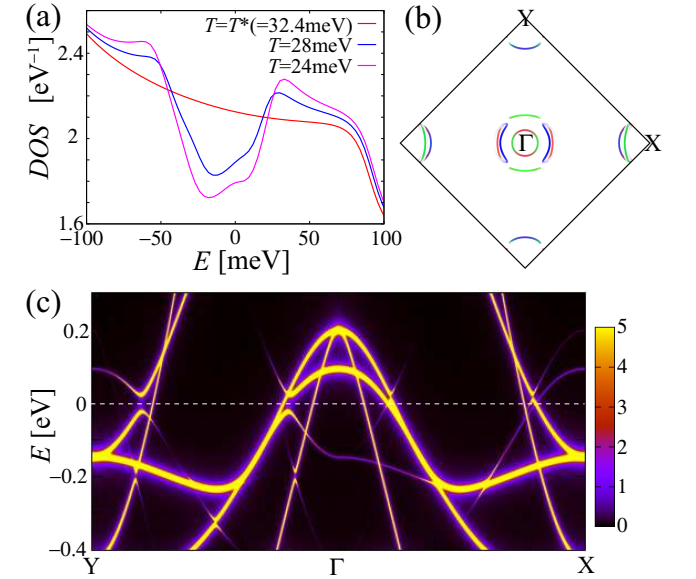


FIG. 4: (a) Energy dependences of DOS at  $T = T^*$  ( $= 32.4\text{meV}$ ),  $28\text{meV}$ , and  $24\text{meV}$  for quasiparticle damping  $\gamma = 10\text{meV}$  in the  $\text{BaFe}_2\text{As}_2$  model. (b) FSs and (c) spectral weight for  $\gamma = 1\text{meV}$  under the  $\mathbf{q} = (0, \pi)$  AFB order at  $T = 28\text{meV}$  in the original two-Fe Brillouin zone.

Here, we discuss the  $\mathbf{q} = (0, \pi)$  AFB ordered state by introducing the mean-field-like  $T$ -dependent form factor  $\hat{f}^{\mathbf{q}}(T) = f^{\max} \tanh \left( 1.74 \sqrt{T^*/T - 1} \right) \hat{f}_{\text{cal}}^{\mathbf{q}}$  for  $T \leq T^*$ .  $\hat{f}_{\text{cal}}^{\mathbf{q}}$  is the calculated form factor at  $T = T^*$ , the maximum absolute value of which is 1. We put  $f^{\max} = 60\text{meV}$ . Figure 4(a) shows the energy dependences of DOS at  $T = T^*$  ( $= 32.4\text{meV}$ ),  $28\text{meV}$ , and

24meV. For  $T < T^*$ , a pseudogap appears, which is consistent with the ARPES measurement [33]. Figures 4(b) and 4(c) show the FSs and spectral weight under the  $\mathbf{q} = (0, \pi)$  AFB order at  $T = 28$ meV, respectively. Here, the folded band structure under the AFB order is unfolded to the original two-Fe Brillouin zone by following Ref. [44]. The unfolded results correspond to the ARPES measurements[33, 34, 45]. The pseudogap originates from the elimination of FS due to the band folding under the  $\mathbf{q} = (0, \pi)$  AFB order. By the band folding, several Dirac-type bandstructures and shadow bands appear, which is consistent with experiments[45].

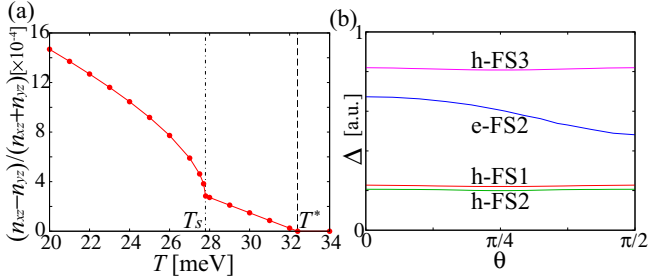


FIG. 5: (a)  $T$  dependence of the nematicity  $\psi = (n_2 - n_3)/(n_2 + n_3)$  including both  $\mathbf{q} = (0, \pi)$  AFB order for  $T < T^*$  and  $\mathbf{q} = \mathbf{0}$  FO order for  $T < T_S$  in the BaFe<sub>2</sub>As<sub>2</sub> model. (b) Superconducting gap function at  $T = 30$ meV given by the nematic fluctuations as a function of the azimuthal angle  $\theta$  on each FS.

Figure 5(a) shows the  $T$  dependence of nematicity  $\psi = (n_2 - n_3)/(n_2 + n_3)$ , where both  $\hat{f}^{(0,\pi)}(T)$  for  $T < T^*$  and the FO order  $\hat{f}^0(T)$  for  $T < T_S$  are introduced. For  $T < T_S$ , we assume  $\hat{f}^0(T) = f_{\text{cal}}^{\max} \tanh(1.74\sqrt{T_S/T - 1}) \hat{f}_{\text{cal}}^0$ , where  $\hat{f}_{\text{cal}}^0$  is the form factor calculated at  $T = T_S$ . Details of the form factor  $\hat{f}_{\text{cal}}^0$  are presented in SM C [39]. We employ  $f^{\max} = 60$ meV, which corresponds to the energy split  $\sim 60$ meV between orbitals 2 and 3 reported in the ARPES measurements [1]. The AFB order does not strongly suppress the FO order transition, as discussed in SM B [39]. These predicted multistage nematic transitions are expected to be realized in Ba122 and NaFeAs families.

The  $T$ -linear behavior  $\psi \propto (T^* - T)$  for  $T_S < T < T^*$  is due to  $\psi \propto [f^{(0,\pi)}(T)]^2$  because the  $f^{(0,\pi)}$ -linear term cannot contribute to the uniform ( $\mathbf{q} = \mathbf{0}$ ) orbital polarization. Therefore,  $\psi$  is independent of the sign of  $f^{(0,\pi)}$ . Note that the form factor  $\hat{f}^{(\pi,0)}$  for  $\mathbf{q} = (\pi, 0)$  gives  $\psi < 0$ . The  $T$ -linear behavior of  $\psi$  below  $T^*$  is consistent with the magnetic torque, X-ray measurements [29] in Ba122, and NMR measurements in Na111[35]. On the other hand,  $\psi \propto \sqrt{T_S - T}$  for  $T < T_S$  is induced by the FO order.

Finally, we discuss mechanism of superconductivity. In our previous paper[16], we proposed the mechanism of  $s_{++}$ -wave mediated by AFB fluctuations. Therein,

we employed the  $\mathbf{k}$ -independent form factor  $\hat{f}^{\mathbf{q}}(\mathbf{k}) = \hat{O}_{\Gamma}$  ( $\Gamma = xz, yz, xy$ ), where  $\hat{O}_{\Gamma}$  is the local charge quadrupole operator. Here, we show that the  $s_{++}$ -wave is realized by the AFB fluctuations by using the form factor obtained microscopically using the DW equation. The pairing interaction  $\hat{V}^{\text{DW}}$  originating from the DW susceptibility  $\chi_{\text{nem}}(\mathbf{q}) \propto (1 - \lambda_{\mathbf{q}})^{-1}$  [28] is expanded by the form factor as

$$V_{l,l',m,m'}^{\text{DW}}(k, k') = \sum_{\mathbf{q}=0, \mathbf{Q}, \mathbf{Q}'} f_{l,l'}^{\mathbf{q}}(\mathbf{k}') \frac{\alpha^{\mathbf{q}}}{1 + \xi_{\mathbf{q}}^2(\mathbf{k} - \mathbf{k}' - \mathbf{q})^2} f_{m',m}^{-\mathbf{q}}(-\mathbf{k}')(3)$$

where  $\alpha^{\mathbf{q}} = \bar{I}^{\mathbf{q}}/(1 - \lambda_{\mathbf{q}})$ , and  $\xi_{\mathbf{q}}$  denotes the correlation length for the  $\mathbf{q}$  DW state. We put  $\xi_{\mathbf{q}} = 1.0$ .  $\bar{I}^{\mathbf{q}}$  is the mean value ( $\hat{f}^{\mathbf{q}}$  basis) of the four-point vertex in the kernel of the DW equation as shown in SM D [39]. We solve the Eliashberg equation including the pairing interaction by using the RPA and  $\hat{V}^{\text{DW}}$ . Figure 5(b) shows the derived  $s_{++}$ -wave gap function  $\Delta$  as a function of the azimuthal angle  $\theta$  from the  $x$  axis on each FS shown in Fig. 1(a). The obtained eigenvalue of the Eliashberg equation is  $\lambda_{\text{SC}} = 3.5$  for  $T = 30$ meV. In this calculation, we employ realistic parameters:  $\alpha_s = 0.96$ ,  $\lambda_{\mathbf{Q}(\mathbf{Q}')} = 0.8$  for the AFB fluctuations,  $\lambda_{\mathbf{0}} = 0.8$  for the FO fluctuations, and  $\bar{I}^{\mathbf{q}} \sim 25$ eV, details of which are presented in SM D [39]. The values of  $\lambda_{\text{SC}}$  should be reduced when the self-energy for Green's function are introduced. We find that the fullgap  $s_{++}$  wave is obtained because the obtained AFB fluctuations with large inter and intra (2–4) orbital components give a sizable inter-FS attractive pairing interaction. Thus, we find that the AFB fluctuations with non-local form factor is a novel mechanism of the  $s_{++}$  wave. The present AFB-fluctuation mechanism is a natural extension of the beyond-Migdal-Eliashberg theory with U-VC developed in Refs. [18, 46]. In future, we will study the mechanism of superconductivity based on the DW fluctuations.

In summary, we studied the origin of the hidden nematic state for  $T_S < T < T^*$  in BaFe<sub>2</sub>As<sub>2</sub>, which is a long-standing unsolved problem. By solving the DW equation, we found that the  $\mathbf{q} = (0, \pi)$  AFB order is the origin of the hidden nematic state. By the AFB order, the  $T$  dependence of the small nematicity  $\psi = (n_{xz} - n_{yz})/(n_{xz} + n_{yz}) \propto (T^* - T)$  observed in the magnetic torque for  $T_S < T < T^*$  as well as the emergence of the pseudogap and shadow band are naturally explained. The phase diagram of Ba122 is understood by the present multistage nematic transitions. In contrast, the hidden nematic order is absent in FeSe, where the  $d_{xy}$ -orbital hole pocket disappears. We also found that the AFB fluctuations favor the superconducting  $s_{++}$ -wave state without sign reversal.

In SM E [39], the present results obtained using the DW equations are verified by the conserving approximation (CA), where the self-energy is introduced in the

Green function  $\hat{G}$ . In the CA framework, the macroscopic conservation laws are satisfied rigorously and unphysical results are avoided.

We are grateful to Y. Yamakawa for useful discussions. This work was supported by the Grants-in-Aid for Scientific Research from MEXT, Japan (No. JP19H05825, JP18H01175, JP17K05543)

---

[1] M. Yi, D. H. Lu, J.-H. Chu, J. G. Analytis, A. P. Sorini, A. F. Kemper, B. Moritz, S.-K. Mo, R. G. Moore, M. Hashimoto, W.-S. Lee, Z. Hussain, T. P. Devereaux, I. R. Fisher, and Z.-X. Shen, *Proc. Natl. Acad. Sci. U.S.A.* **108**, 6878 (2011).

[2] M. Yoshizawa, D. Kimura, T. Chiba, S. Simayi, Y. Nakanishi, K. Kihou, C.-H. Lee, A. Iyo, H. Eisaki, M. Nakajima, and S. Uchida, *J. Phys. Soc. Jpn.* **81**, 024604 (2012).

[3] A. E. Böhmer, P. Burger, F. Hardy, T. Wolf, P. Schweiss, R. Fromknecht, M. Reinecker, W. Schranz, and C. Meingast, *Phys. Rev. Lett.* **112**, 047001 (2014).

[4] Y. Gallais, R. M. Fernandes, I. Paul, L. Chauviere, Y.-X. Yang, M.-A. Measson, M. Cazayous, A. Sacuto, D. Colson, and A. Forget, *Phys. Rev. Lett.* **111**, 267001 (2013).

[5] Y. Hu, X. Ren, R. Zhang, H. Luo, S. Kasahara, T. Watashige, T. Shibauchi, P. Dai, Y. Zhang, Y. Matsuda, and Y. Li, *Phys. Rev. B* **93**, 060504(R) (2016).

[6] R. M. Fernandes, L. H. VanBebber, S. Bhattacharya, P. Chandra, V. Keppens, D. Mandrus, M. A. McGuire, B. C. Sales, A. S. Sefat, and J. Schmalian, *Phys. Rev. Lett.* **105**, 157003 (2010).

[7] R. M. Fernandes, E. Abrahams, and J. Schmalian, *Phys. Rev. Lett.* **107**, 217002 (2011).

[8] F. Wang, S. A. Kivelson, and D.-H. Lee, *Nat. Phys.* **11**, 959 (2015).

[9] R. Yu, and Q. Si, *Phys. Rev. Lett.* **115**, 116401 (2015).

[10] J. K. Glasbrenner, I. I. Mazin, H. O. Jeschke, P. J. Hirschfeld, and R. Valenti, *Nat. Phys.* **11**, 953 (2015).

[11] C. Fang, H. Yao, W.-F. Tsai, J. P. Hu, and S. A. Kivelson, *Phys. Rev. B* **77**, 224509 (2008).

[12] R. M. Fernandes and A. V. Chubukov, *Rep. Prog. Phys.* **80**, 014503 (2017).

[13] F. Krüger, S. Kumar, J. Zaanen, J. van den Brink, *Phys. Rev. B* **79**, 054504 (2009).

[14] W. Lv, J. Wu, and P. Phillips, *Phys. Rev. B* **80**, 224506 (2009).

[15] C.-C. Lee, W.-G. Yin, and W. Ku, *Phys. Rev. Lett.* **103**, 267001 (2009).

[16] H. Kontani, T. Saito, and S. Onari, *Phys. Rev. B* **84**, 024528 (2011).

[17] S. Onari and H. Kontani, *Phys. Rev. Lett.* **109**, 137001 (2012).

[18] S. Onari, Y. Yamakawa, and H. Kontani, *Phys. Rev. Lett.* **112**, 187001 (2014).

[19] S. Onari, Y. Yamakawa, and H. Kontani, *Phys. Rev. Lett.* **116**, 227001 (2016).

[20] Y. Yamakawa, S. Onari and H. Kontani, *Phys. Rev. X* **6**, 021032 (2016).

[21] S. Onari and H. Kontani, *Iron-Based Superconductivity*, (ed. P.D. Johnson, G. Xu, and W.-G. Yin, Springer-Verlag Berlin and Heidelberg GmbH & Co. K (2015)).

[22] K. Jiang, J. Hu, H. Ding, and Z. Wang, *Phys. Rev. B* **93**, 115138 (2016).

[23] L. Fanfarillo, G. Giovannetti, M. Capone, and E. Bascones, *Phys. Rev. B* **95**, 144511 (2017).

[24] A. V. Chubukov, M. Khodas, and R. M. Fernandes, *Rhys. Rev. X* **6**, 041045 (2016).

[25] J. Li, D. Zhao, Y. P. Wu, S. J. Li, D. W. Song, L. X. Zheng, N. Z. Wang, X. G. Luo, Z. Sun, T. Wu, and X. H. Chen, arXiv:1611.04694.

[26] X. Liu, R. Tao, M. Ren, W. Chen, Q. Yao, T. Wolf, Y. Yan, T. Zhang, and D. Feng, *Nat. Commun.* **10**, 1039 (2019).

[27] K. Ishida, M. Tsujii, S. Hosoi, Y. Mizukami, S. Ishida, A. Iyo, H. Eisaki, T. Wolf, K. Grube, H. v. Löhneysen, R. M. Fernandes, and T. Shibauchi, arXiv:1812.05267.

[28] S. Onari and H. Kontani, *Phys. Rev. B* **100**, 020507(R) (2019).

[29] S. Kasahara, H. J. Shi, K. Hashimoto, S. Tonegawa, Y. Mizukami, T. Shibauchi, K. Sugimoto, T. Fukuda, T. Terashima, Andriy H. Nevidomskyy, and Y. Matsuda, *Nature* **486**, 382 (2012).

[30] Y. K. Kim, W. S. Jung, G. R. Han, K.-Y. Choi, C.-C. Chen, T. P. Devereaux, A. Chainani, J. Miyawaki, Y. Takata, Y. Tanaka, M. Oura, S. Shin, A. P. Singh, H. G. Lee, J.-Y. Kim, and C. Kim, *Phys. Rev. Lett.* **111**, 217001 (2013).

[31] E. Thewalt, I. M. Hayes, J. P. Hinton, A. Little, S. Patankar, L. Wu, T. Helm, C. V. Stan, N. Tamura, J. G. Analytis, and J. Orenstein, *Phys. Rev. Lett.* **121**, 027001 (2018).

[32] T. Shimojima *et al.*, unpublished.

[33] T. Shimojima *et al.*, *Phys. Rev. B* **89**, 045101 (2014).

[34] T. Shimojima, W. Malaeb, A. Nakamura, T. Kondo, K. Kihou, C.-H. Lee, A. Iyo, H. Eisaki, S. Ishida, M. Nakajima, S. Uchida, K. Ohgushi, K. Ishizaka, and S. Shin, *Sci. Adv.* **3**, e1700466 (2017).

[35] R. Zhou, L. Y. Xing, X. C. Wang, C. Q. Jin, and G.-Q. Zheng, *Phys. Rev. B* **93**, 060502(R) (2016).

[36] X. Ren, L. Duan, Y. Hu, J. Li, R. Zhang, H. Luo, P. Dai, and Y. Li, *Phys. Rev. Lett.* **115**, 197002 (2015).

[37] H. Man, R. Zhang, J. T. Park, X. Lu, J. Kulda, A. Ivanov, and P. Dai, *Phys. Rev. B* **97**, 060507(R) (2018).

[38] H. Nakaoka, Y. Yamakawa, and H. Kontani, *Phys. Rev. B* **98**, 125107 (2018).

[39] Supplemental Material

[40] T. Miyake, K. Nakamura, R. Arita, and M. Imada, *J. Phys. Soc. Jpn.* **79**, 044705 (2010).

[41] K. Kawaguchi, M. Tsuchiizu, Y. Yamakawa, and H. Kontani, *J. Phys. Soc. Jpn.* **86**, 063707 (2017).

[42] T. Shimojima, Y. Suzuki, T. Sonobe, A. Nakamura, M. Sakano, J. Omachi, K. Yoshioka, M. Kuwata-Gonokami, K. Ono, H. Kumigashira, A. E. Böhmer, F. Hardy, T. Wolf, C. Meingast, H. v. Löhneysen, H. Ikeda, and K. Ishizaka, *Phys. Rev. B* **90**, 121111(R) (2014).

[43] R.-Q. Xing, L. Classen, A. V. Chubukov, *Phys. Rev. B* **98**, 041108 (2018).

[44] W. Ku, T. Berlijn, and C.-C. Lee, *Phys. Rev. Lett.* **104**, 216401 (2010).

[45] A. Fujimori, private communication.

[46] R. Tazai and H. Kontani, *Phys. Rev. B* **98**, 205107 (2018).

[Supplementary Material]

Hidden antiferro-nematic order in Fe-based superconductor  $\text{BaFe}_2\text{As}_2$  and  $\text{NaFeAs}$  above  $T_S$

Seiichiro Onari and Hiroshi Kontani

*Department of Physics, Nagoya University, Nagoya 464-8602, Japan*

**A: Eight-orbital models for  $\text{BaFe}_2\text{As}_2$  and FeSe**

Here, we introduce the eight-orbital  $d$ - $p$  models for  $\text{BaFe}_2\text{As}_2$  and FeSe that are analyzed in the main text. We first derive first-principles tight-binding models by using the WIEN2k and WANNIER90 codes. Next, to obtain the experimentally observed Fermi surfaces (FSs) in FeSe, we introduce the  $k$ -dependent shifts for orbital  $l$ ,  $\delta E_l$ , by introducing the intra-orbital hopping parameters, as explained in Ref. [1]. We shift the  $d_{xy}$ -orbital band [ $d_{xz/yz}$ -orbital band] at  $(\Gamma, M, X)$  points by  $(-0.6, -0.25, +0.24)$  [ $(-0.24, 0, +0.12)$ ] for FeSe. We also introduce the mass enhancement factor  $z^{-1} = 1.6$  for  $d_{xy}$  orbital in the FeSe model.

Figure S1 shows the bandstructures of the obtained  $\text{BaFe}_2\text{As}_2$  model and FeSe model.

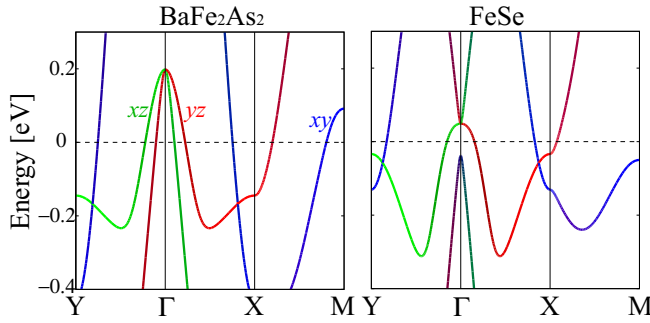


FIG. S1: Obtained bandstructures of the  $\text{BaFe}_2\text{As}_2$  model and FeSe model. The colors green, red and blue correspond to orbitals 2, 3 and 4, respectively.

Next, we explain the multiorbital Coulomb interaction. The bare Coulomb interaction for the spin channel in the main text is

$$(\Gamma^s)_{l_1 l_2, l_3 l_4} = \begin{cases} U_{l_1, l_1}, & l_1 = l_2 = l_3 = l_4 \\ U'_{l_1, l_2}, & l_1 = l_3 \neq l_2 = l_4 \\ J_{l_1, l_3}, & l_1 = l_2 \neq l_3 = l_4 \\ J_{l_1, l_2}, & l_1 = l_4 \neq l_2 = l_3 \\ 0, & \text{otherwise.} \end{cases} \quad (\text{S1})$$

Furthermore, the bare Coulomb interaction for the

charge channel is

$$(\hat{\Gamma}^c)_{l_1 l_2, l_3 l_4} = \begin{cases} -U_{l_1, l_1}, & l_1 = l_2 = l_3 = l_4 \\ U'_{l_1, l_2} - 2J_{l_1, l_2}, & l_1 = l_3 \neq l_2 = l_4 \\ -2U'_{l_1, l_3} + J_{l_1, l_3}, & l_1 = l_2 \neq l_3 = l_4 \\ -J_{l_1, l_2}, & l_1 = l_4 \neq l_2 = l_3 \\ 0, & \text{otherwise.} \end{cases} \quad (\text{S2})$$

Here,  $U_{l, l}$ ,  $U'_{l, l'}$  and  $J_{l, l'}$  denote the first-principles Coulomb interaction terms for  $d$ -orbitals of  $\text{BaFe}_2\text{As}_2$  given in Ref. [2].

By using the multiorbital Coulomb interaction, the spin (charge) susceptibility in the RPA is given by

$$\hat{\chi}^{s(c)}(q) = \hat{\chi}(q)[1 - \hat{\Gamma}^{s(c)}\hat{\chi}^0(q)]^{-1}, \quad (\text{S3})$$

where the irreducible susceptibility is

$$\chi_{l, l'; m, m'}^0(q) = -\frac{T}{N} \sum_k G_{l, m}(k + q) G_{m', l'}(k). \quad (\text{S4})$$

Here,  $\hat{G}(k)$  is the multiorbital Green function introduced in the main text.

The kernel function  $\hat{K}^q(k, k')$  [3, 4] is given by

$$K_{l, l'; m, m'}^q(k, k') = - \sum_{m_1, m_2} I_{l, l'; m_1, m_2}^q(k, k') g_{m_1, m_2; m, m'}^q(k'), \quad (\text{S5})$$

where  $g_{l, l'; m, m'}^q(k) \equiv G_{l, m}(k + \mathbf{q}) G_{m', l'}(k)$ , and  $\hat{I}^q(k, k')$  is the four-point vertex.

$\hat{I}^q(k, k')$  is given as

$$\begin{aligned} I_{l, l'; m, m'}^q(k, k') = & \sum_{b=s, c} \left[ -\frac{a^b}{2} V_{l, m; l', m'}^b(k - k') \right. \\ & + \frac{T}{N} \sum_{p, l_1, l_2, m_1, m_2} \frac{a^b}{2} V_{l, l_1; l_2, m'}^b(p + \mathbf{q}) V_{m_2, m; l', m_1}^b(p) \\ & \times G_{l_1, m_1}(k - p) G_{l_2, m_2}(k' + p + \mathbf{q}) \\ & + \frac{T}{N} \sum_{p, l_1, l_2, m_1, m_2} \frac{a^b}{2} V_{l, l_1; m, m_2}^b(p + \mathbf{q}) V_{m', l_2; l', m_1}^b(p) \\ & \left. \times G_{l_1, m_1}(k - p) G_{l_2, m_2}(k' - p) \right], \end{aligned} \quad (\text{S6})$$

where  $a^s = 3$ ,  $a^c = 1$ ,  $p = (\mathbf{p}, \omega_l)$ , and  $\hat{V}^{s(c)}(q) = \hat{\Gamma}^{s(c)} + \hat{\Gamma}^{s(c)}\hat{\chi}^{s(c)}(q)\hat{\Gamma}^{s(c)}$ .

In Eq. (S6), the first line corresponds to the Mak-Thompson (MT) term, and the second and third lines give the AL1 and AL2 terms, respectively. In the MT term, the first-order term with respect to  $\hat{\Gamma}^{s,c}$  gives the Hartree-Fock (HF) term in the mean-field theory.

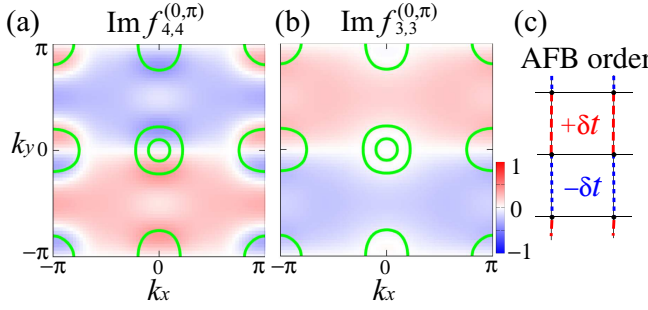


FIG. S2: Sub-dominant form factors for  $\mathbf{q} = (0, \pi)$  on (a) orbital 4 and (b) orbital 3. (c) Schematic picture of  $\mathbf{q} = (0, \pi)$  intra-orbital AFB order.

### B: Form factor for $\mathbf{q} = (0, \pi)$

Here, we explain the obtained  $\mathbf{q} = (0, \pi)$  form factor in  $\text{BaFe}_2\text{As}_2$ . Figures S2 (a) and (b) show the sub-dominant form factors  $f_{4,4}^{\mathbf{q}}$  and  $f_{3,3}^{\mathbf{q}}$  for  $\mathbf{q} = (0, \pi)$ . We see that  $f_{4,4}^{\mathbf{q}}$  in Fig. 3 dominates over these components. As shown Fig. S2 (c),  $f_{4,4}^{\mathbf{q}}$  and  $f_{3,3}^{\mathbf{q}}$  correspond to the intra-orbital AFB order with the modulation of correlation hopping  $\pm\delta t$  along the  $y$  direction, respectively.

Next, we show the obtained results under the AFB ordered state for  $T < T^*$  in the  $\text{BaFe}_2\text{As}_2$  model. We introduce the  $\mathbf{q} = (0, \pi)$  AFB order in the same way as in the main text:  $\hat{f}^{\mathbf{q}}(T) = f^{\max} \tanh\left(1.74\sqrt{T^*/T - 1}\right) \hat{f}_{\text{cal}}^{\mathbf{q}}$  for  $T \leq T^*$ . Figure S3 shows the  $T$  dependence of  $\alpha_s$  with and without  $\hat{f}^{\mathbf{q}}(T)$ . The AFB order suppresses  $\alpha_s$  just slightly, similarly to the result of  $\lambda_0$  in Fig. 2(a). Thus, neither  $\chi_{\text{nem}}(\mathbf{0}) \propto 1/(1 - \lambda_0)$  or spin fluctuations  $\chi^s \propto 1/(1 - \alpha_s)$  shows a sizable anomaly at  $T = T^*$ , which is consistent with experiments. In contrast, the FO order at  $T = T_S$  causes a sizable anomaly for  $\chi_{\text{nem}}(\mathbf{0})$  and  $\chi_s$ .

The single-component GL theory considering terms up to the sixth order[5] predicts the second-order transition at  $T = T^*$  and the meta-nematic transition at  $T = T_S$ . In the present theory, in contrast, both transitions are second-order owing to the multi-orbital component of the form factor. In addition, the  $T$ -linear dependence of  $\psi$  for  $T_S < T < T^*$  is naturally explained by the AFB order in our theory.

### C: Form factor of FO order

Here, we explain the obtained  $\mathbf{q} = \mathbf{0}$  form factor in  $\text{BaFe}_2\text{As}_2$ . Figures S4 (a) and (b) show the dominant form factor for  $\mathbf{q} = \mathbf{0}$ .  $f_{4,4}^{\mathbf{0}} \propto \cos k_x - \cos k_y$  corresponds to the  $B_{1g}$  bond order of orbital 4 as shown in Fig. S4 (c). Figure S4 (b) shows  $f_{3,3}^{\mathbf{0}}(k_x, k_y) = -f_{2,2}^{\mathbf{0}}(-k_y, k_x)$ , which causes the  $B_{1g}$  FO order  $n_2 > n_3$  in Fig. S4 (d). Note that the  $f_{3,3}^{\mathbf{0}} \propto \cos k_x - \cos k_y$  component is also

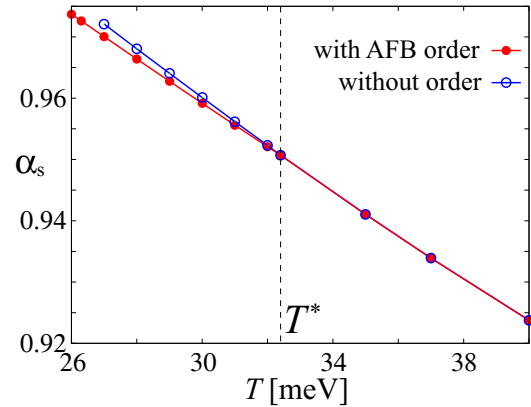


FIG. S3:  $T$  dependencies of  $\alpha_s$  with and without the AFB order in the  $\text{BaFe}_2\text{As}_2$  model.

obtained, which corresponds to the  $B_{1g}$  bond order of orbital 3 as shown in Fig. S4 (c).

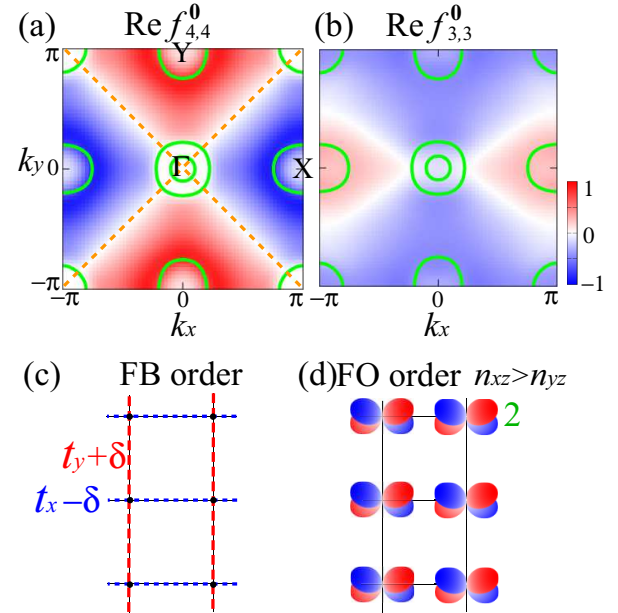


FIG. S4: Form factors at  $\mathbf{q} = \mathbf{0}$  obtained as the second-largest eigenvalue in the  $\text{BaFe}_2\text{As}_2$  model on (a) orbital 4 and (b) orbital 3. The green lines denote FSs without the self-energy. The form factor for orbital 4,  $f_{4,4}^{\mathbf{0}} \propto \cos k_x - \cos k_y$ , results in the ferro-bond (FB) order. Schematic pictures of (c) FB order due to  $f_{4,4}^{(0, \pi)}$  and (d) FO order due to  $f_{3,3}^{\mathbf{0}}$ .

### D: Pairing interaction by the DW fluctuations

Here, we explain the formulation for analyzing the superconducting state. We solve the following Eliashberg equation, which includes the RPA pairing interaction and the DW fluctuation pairing interaction  $\hat{V}^{\text{DW}}$  with the

cutoff energy  $W_c = 0.02\text{eV}$ :

$$\begin{aligned} \lambda_{\text{SC}}\Delta_{l,m}(k) &= \frac{T}{N} \sum_{k'} \sum_{l',l'',m',m''} \left[ -\frac{3}{2}\hat{V}^s(k-k') + \frac{1}{2}\hat{V}^c(k-k') \right. \\ &\quad \left. + \hat{V}^{\text{DW}}(k,k') + \frac{1}{2}(\hat{\Gamma}^c - \hat{\Gamma}^s) \right]_{l,l';m',m} \\ &\quad \times G_{l',l''}(k')G_{m',m''}(-k')\Delta_{l'',m''}(k'). \end{aligned} \quad (\text{S7})$$

$\hat{V}^{\text{DW}}$  in Eq. (3) is composed of  $\alpha^q = \bar{I}^q/(1 - \lambda_q)$ , where  $\bar{I}^q$  is the mean value of  $\hat{I}^q$  in the basis of  $\hat{f}'^q(\mathbf{k}') \equiv \hat{f}^q(\mathbf{k}' - \mathbf{q}/2)$  and is given as

$$\bar{I}^q = \frac{\sum_{\mathbf{k}'} \sum_{l,l',m,m'} f_{l',l}^{q,-q}(\mathbf{k}') I_{l,l';m,m'}^q(\mathbf{k}', -\mathbf{k}') f_{m,m'}^{q,q}(-\mathbf{k}')}{\sum_{\mathbf{k}'} \sum_{l,l',m,m'} f_{l',l}^{q,-q}(\mathbf{k}') f_{l,l'}^{q,q}(\mathbf{k}') f_{m,m'}^{q,q}(-\mathbf{k}') f_{m',m}^{q,-q}(-\mathbf{k}')}. \quad (\text{S8})$$

By summing  $\mathbf{k}'$  on the FSs, we obtain  $\bar{I}^0 = 28\text{eV}$  at  $T = 30\text{meV}$  for the microscopically calculated form factor in the  $\text{BaFe}_2\text{As}_2$  model. Because of large  $\bar{I}^q/U \sim 10$ , the AFB fluctuations give large attractive pairing interaction. The obtained enhancement of  $\bar{I}^q$  is consistent with the large U-VC introduced in beyond-Migdal-Eliashberg theory in Refs.[6, 7].

Note that  $\hat{I}^q(k, k')$  is large only at low energies on FSs, which is similar to the U-VC. In fact, mean value of  $\hat{I}^q(k, k')$  in Brillouin zone (local approximation) is small  $\sim 1\text{eV}$ . Since the superconductivity is low energy physics on FSs, the large DW fluctuation pairing interactions induce high  $T_c$ .

In future, we will study the mechanism of superconductivity based on the DW fluctuations. While we studied the superconductivity mediated by the orbital fluctuations in Refs. [6–8], we can calculate superconductivity mediated by both orbital fluctuations and bond fluctuations by using the present theory.

### E: Conserving approximation

In the main text, we employ the RPA, in which the self-energy is not included in the spin (charge) susceptibility  $\hat{\chi}^{s(c)}$  and kernel function  $\hat{K}^q(k, k')$ . For this reason, the DW equation in the RPA violates the conserving-approximation (CA) formalism of Baym and Kadanoff[9]. The great merit of CA is that it rigorously satisfies the macroscopic conservation laws. This merit is important to avoid unphysical results. Here, we first calculate the one-loop self-energy by using the fluctuation exchange (FLEX) approximation[3, 10]. Next, we solve the DW equation including the FLEX self-energy to satisfy the CA formalism.

The FLEX self-energy ( $C_4$ ) is given by  $\hat{\Sigma}(k) = \frac{T}{N} \sum_q \hat{V}^\Sigma(q) \hat{G}(k-q)$ , where  $\hat{G}(k) = [(i\epsilon_n - \mu)\hat{1} - \hat{h}^0(\mathbf{k}) - \hat{\Sigma}(k)]^{-1}$  is the Green function with the self-energy, and  $\hat{V}^\Sigma$  is the interaction matrix for the self-energy.  $\hat{V}^\Sigma$  is

given as

$$\begin{aligned} \hat{V}^\Sigma &= \frac{3}{2}\hat{\Gamma}^s\hat{\chi}^s(q)\hat{\Gamma}^s + \frac{1}{2}\hat{\Gamma}^c\hat{\chi}^c(q)\hat{\Gamma}^c \\ &\quad - \frac{1}{2}[\hat{\Gamma}^c\hat{\chi}^0(q)\hat{\Gamma}^c + \hat{\Gamma}^s\hat{\chi}^0(q)\hat{\Gamma}^s] \\ &\quad - \frac{1}{4}(\hat{\Gamma}^s + \hat{\Gamma}^c)\hat{\chi}^0(q)(\hat{\Gamma}^s + \hat{\Gamma}^c). \end{aligned} \quad (\text{S9})$$

We solve  $\hat{\Sigma}$ ,  $\hat{G}$ , and  $\hat{\chi}^{s(c)}$  self-consistently. By introducing the obtained functions, we improve the kernel of the DW equation in Eq. (S5) and (S6) and solve the symmetry-breaking self-energy (form factor) in the framework of CA.

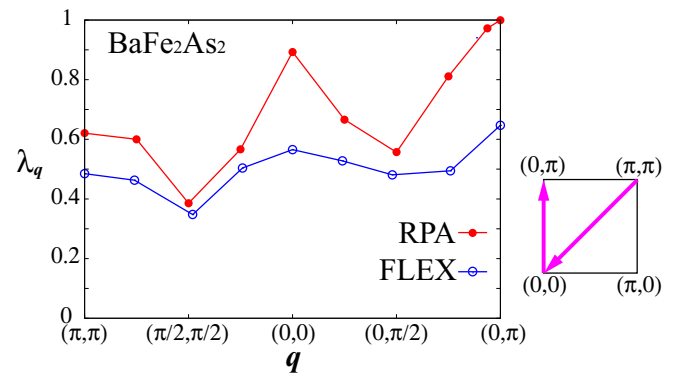


FIG. S5:  $\mathbf{q}$  dependences of  $\lambda_q$  obtained using the RPA at  $T = T^*$  ( $\alpha_s = 0.951$ ) and the FLEX approximation at  $T = 5\text{meV}$  ( $\alpha_s = 0.945$ ,  $r = 0.680$ ) in the  $\text{BaFe}_2\text{As}_2$  model. The  $\mathbf{q}$  path is shown by arrows in the right panel.

Figure S5 shows the  $\mathbf{q}$  dependences of  $\lambda_q$  obtained using the RPA at  $T = T^* = 32.4\text{meV}$  ( $\alpha_s = 0.951$ ) and the FLEX approximation at  $T = 5\text{meV}$  ( $\alpha_s = 0.945$ ,  $r = 0.680$ ). In the FLEX approximation, we take  $N = 100 \times 100$   $\mathbf{k}$ -meshes and 1024 Matsubara frequencies. The result of the FLEX approximation is similar to that of RPA employed in the main text. The AFB order  $f^{(0,\pi)}$  is dominant over the FO order  $f^0$ . Thus, the results in the main text are verified in the CA framework. Although we cannot calculate for larger values of  $r$  and  $\alpha_s$  because of the insufficiency of frequency- and  $\mathbf{k}$ -mesh numbers, the value of  $\lambda_q$  will reach unity for larger values of  $r$  and  $\alpha_s$ .

---

- [1] Y. Yamakawa, S. Onari and H. Kontani, Phys. Rev. X **6**, 021032 (2016).
- [2] T. Miyake, K. Nakamura, R. Arita, and M. Imada, J. Phys. Soc. Jpn. **79**, 044705 (2010).
- [3] S. Onari, Y. Yamakawa, and H. Kontani, Phys. Rev. Lett. **116**, 227001 (2016).
- [4] K. Kawaguchi, M. Tsuchizawa, Y. Yamakawa, and H. Kontani, J. Phys. Soc. Jpn. **86**, 063707 (2017).

- [5] S. Kasahara, H. J. Shi, K. Hashimoto, S. Tonegawa, Y. Mizukami, T. Shibauchi, K. Sugimoto, T. Fukuda, T. Terashima, Andriy H. Nevidomskyy, and Y. Matsuda, *Nature* **486**, 382 (2012).
- [6] S. Onari, Y. Yamakawa, and H. Kontani, *Phys. Rev. Lett.* **112**, 187001 (2014).
- [7] R. Tazai and H. Kontani, *Phys. Rev. B* **98**, 205107 (2018).
- [8] Y. Yamakawa, S. Onari and H. Kontani, arXiv:1911.00363.
- [9] G. Baym and P. Kadanoff, *Phys. Rev.* **124**, 287 (1961).
- [10] N. E. Bickers and S. R. White, *Phys. Rev. B* **43**, 8044 (1991).